# Delayed fracture caused by time-dependent damage in PDMS

Jikun Wang<sup>a,1</sup>, Bangguo Zhu<sup>b,1</sup>, Chung-Yuen Hui<sup>b,c,\*</sup>, Alan T. Zehnder<sup>b,\*</sup>

<sup>a</sup>Sibley School of Mechanical and Aerospace Engineering, Cornell University, Ithaca, NY 14853, USA
<sup>b</sup>Sibley School of Mechanical and Aerospace Engineering, Field of Theoretical and Applied Mechanics, Cornell
University, Ithaca, New York, 14853, USA
<sup>c</sup>Global Station for Soft Matter, GI-CoRE, Hokkaido University, Sapporo 001-0021, Japan

#### Abstract

An experimental and theoretical study of delayed fracture of polydimethlsiloxane (PDMS) is presented. Previous works have demonstrated that delayed fracture in single edge notch specimens is caused by time dependent damage due to chain scission. Here we study the interactions between damage and the elastic field using different specimens and crack geometries with blunt and sharp cracks. Our experiments show that initial toughness is not well defined, as stable slow crack growth can occur over a range of applied loads. Our experiments demonstrate that there is a universal relation between crack growth rate and applied energy release rate. A model coupling the nonlinear elastic deformation and rate dependent bond scission is proposed and is in good agreement with experimental data.

Keywords: delayed fracture, crack growth, catastrophic failure, PDMS, time-dependent damage

# 1. Introduction

The simplest mechanical test for materials is to stretch a bar under uniaxial tension. The stress or strain when the material breaks is known as fracture strength or elongation at failure. Although fracture strength or elongation is easy to measure, it can vary greatly from specimen to specimen and is sensitive to size and loading rate [1, 2]. The fracture mechanics approach mediates the first of these difficulties by testing a pre-cracked specimen and using the critical energy release rate,  $G_c$ , at crack initiation as a criterion for failure. For time independent elastic solids,  $G_c$  is a well-defined material property. One key advantage of the fracture mechanics approach is that while the fracture strength is geometry dependent,  $G_c$  is not [3, 4].

However, for many soft materials,  $G_c$  is not well defined [5, 6, 7, 8](a detailed discussion of the meaning of toughness will be given here). For example, loading materials below their fracture strength or  $G_c$  does not necessarily mean they are safe [5, 9, 10]. When the external loading is below the critical criteria, instead of instantaneously breaking, catastrophic fracture due to the

<sup>\*</sup>Corresponding author

Email addresses: ch45@cornell.edu (Chung-Yuen Hui), atz2@cornell.edu (Alan T. Zehnder)

<sup>&</sup>lt;sup>1</sup>Contributed equally

initiation and rapid propagation of a macroscopic crack (in samples with no pre-crack) or slow crack growth may occur. This time dependent phenomenon is called delayed fracture (DF) and has been observed in ceramics [11], metals [12], plastics [13] and soft materials such as hydrogels and elastomers [14, 15, 16, 17, 18].

Studies of DF are difficult to carry out since: (1) DF, being a time dependent phenomenon, is sensitive to loading history. For example, the behavior of a sample in a relaxation test [19] can be markedly different than the same sample in a creep or constant strain rate test [17]. (2) DF is extremely sensitive to stress concentration, and hence sample geometry can significantly affect behavior. A small decrease in applied stress/strain may increase the delay time by orders of magnitude, from seconds to hours [5, 9]. Here we note that in the literature, DF has been studied using different specimens with varying degree of stress concentration. For example, some studies use samples with sharp crack tips [5, 10, 16], while others use blunted cracks or notches with finite radius (usually in the scale of 0.1mm) [9, 18, 20]. In some studies, tension samples with no precrack are used [14, 17]. (3) There can be many time dependent mechanisms underlying DF, e.g., poroelasticity [5, 10], viscoelasticity [17, 21] or damage due to rate dependent bond breaking [22]. For example, in hydrogels, movement of solvent can change the energy release rate near the crack tip and can lead to catastrophic fracture when the energy release rate exceeds the toughness [5, 18]. In highly viscoelastic hydrogels such as Polyampholyte gels [23], creep rupture (DF in some literature) is intimately associated with viscoelasticity, which is controlled by the breaking and healing kinetics of ionic bonds as well as the degree of chemical crosslinking [17]. Whether these mechanisms are strongly coupled depends on the material system, loading history and geometry. Due to these difficulties, there are considerable variations in observation: in some work slow crack growth is observed before catastrophic failure [16, 18, 21], while in others only catastrophic failure is observed [5, 9, 10, 14].

The choice of experiments in this work is directed by these considerations. To study the effect of loading histories on DF, we used both relaxation and constant strain rate tests. The relaxation test is particularly relevant since in contrast to the constant strain rate test, there is no energy input to the specimen during the hold period prior to DF. To address the effect of specimen geometry on DF, we use two geometries: a pure shear (PS) and a double-edge crack (DEC) sample. From these two geometries, we can generate different specimens by varying the crack length and the sharpness of the crack tip. Finally, since our main interest is DF in soft materials, we chose PDMS, a widely used silicon-based polymer as our model system. When cross-linked at a ratio of 10 to 1, PDMS is an elastomer, with a small amount of viscoelasticity and is used in many applications such as soft robots, substrates in microfluidic and microelectromechanical devices.

We mention two closely related studies on the DF behavior of PDMS. The first used a laser speckle strain imaging technique to study the DF of a single edge notch sample [9]. The second,

more recent, combines multi-speckle diffusing wave spectroscopy technique, mechanophore mapping of chain scission and digital image correlation (DIC) to probe the mechanism of DF of single edge crack sample [8]. Both works presented strong evidence that the microscopic origin of DF is localized molecular damage due to chain scission. In addition, both experiments showed that a fracture precursor in the form of a region of enhanced dynamics localized near the notch or crack tip. As noted by Ju et al.[8], this region of enhanced dynamics can be very large, on the order of  $0.01mm^2$ . An interesting result is that both studies observed very rapid crack growth once fracture initiates [8, 9].

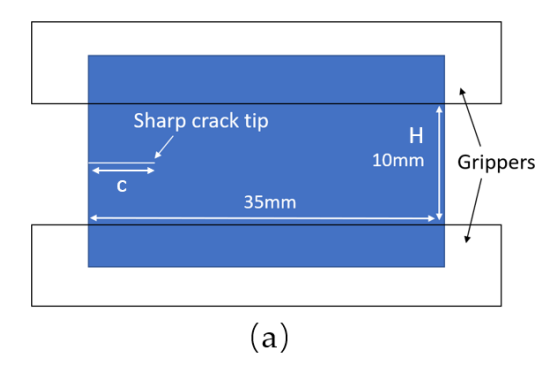
The primary focus of this work is to experimentally study the interaction between localized damage and the elastic field, by controlling the elastic fields using two different crack samples with different crack geometries (short or long crack, crack with blunt tips to reduce stress concentration) as well as loading histories (relaxation and constant stretch rate test). This coupling of elastic fields and local damage reveals a wide range of DF behavior. For example, DF can occur in the form of slow and stable crack growth (the slowest crack growth rate is on the order of 1nm/s) over a wide range of energy release rates, from  $35J/m^2$  to  $220J/m^2$ . On the other hand, a simple change of crack or sample geometry can lead to rapid catastrophic failure once fracture initiates.

The plan of this paper is as follows. The experimental setup for DF testing and material synthesis is given in section 2. Section 3 presents experimental results for blunted and sharp crack samples. Here we introduce the concept of small scale damage and G (energy release rate) controlled crack growth and demonstrate experimentally that there is a universal relation between crack growth rate, v, and energy release rate, G. In section 4 we present an analytic model based on chain breaking kinetics to determine the relation between v and G and compare the prediction of this model with experiments. Section 5 is summary and discussion. The concept of toughness is revisited in the discussion.

### 2. Samples and experimental design

Our experiments use two types of crack specimens (pure shear (PS) (Fig. 1 (a)) and double edge crack (DEC) (Fig. 1 (b))) with different crack geometries. The thickness of all specimens is 0.55mm thus plane stress conditions prevail. The crack tips in PS specimens are sharp whereas those in DEC specimens are blunted with a finite crack tip radius of 0.25mm (the circular hole at the crack tip is drilled by a CNC router with 0.25mm cutter, the spinning rate is 10000 rpm). Our choice of specimens is based on the observation that sharp cracks tend to initiate and grow slowly under quasi-static conditions. PS specimens allow us to study steady state crack growth in a relaxation test where the displacement is fixed on the PS sample (see Fig. 1 (a)).

For sharp crack samples, the crack is cut using a razor blade, with the cutting edge towards the crack tip. To ensure initial sharpness, we first stretch the PS sample slowly  $(10^{-4}/s)$  until the crack



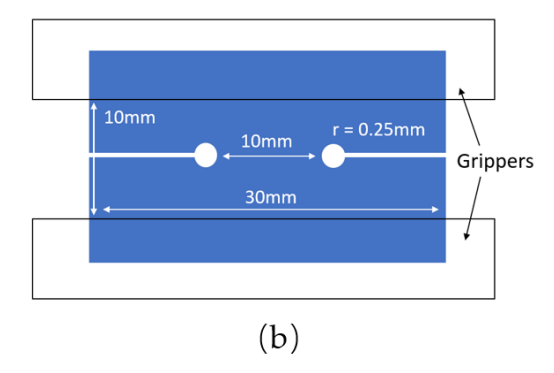


Figure 1: Samples for delayed fracture. (a) Pure shear (PS) sample with sharp crack tip. (b) Double edge crack (DEC) sample with blunt crack tip. The radius of the hole is 0.25mm.

propagates a very small amount, and then unload the sample to zero stretch. After this cycle the crack is very sharp because a new crack tip was generated during crack propagation. In Fig. 1 (a) the crack length is not specified, because samples with different initial crack lengths will be used in this study. We will specify the length of the crack when we discuss our experimental results.

Fracture testing, Relaxation test: For DF tests, we stretched the samples with a stretch rate of 0.1/s until the designated displacement. The nominal stretch ratio associated with this displacement is denoted by  $\lambda$ , which will be called the applied stretch ratio. Then the displacements were fixed at the grips, during which the force was recorded using a load cell (Interface, SMT1-100N) and images were acquired using a camera (FLIR Grasshopper 3 4.1 MP Mono) at 20 fps.

**DIC implementation:** DIC was used to monitor the change of strain field for tension and relaxation tests. Details of the DIC measurements are given in section S3 of the supporting information.

## 3. Experimental results

# 3.1. Delayed fracture for blunt crack DEC sample

To determine the stretch levels to use in the DF experiments, we first stretched the sample with stretch rate 0.0001/s until it breaks. The fracture stretch for this sample was between 1.65 to 1.7. Based on this value, in the relaxation experiments, we stretched the sample with a stretch rate of 0.1/s to a stretch of 1.6 and then held the displacement. During the holding period, images are acquired for DIC analysis. An example is shown in Fig. 2.

We observed two interesting phenomena. The first is shown in Fig. 3(a) where the relative stretch ratio at a fixed point  $(100\mu m)$  ahead of the crack tip, measured over a  $20\mu m \times 20\mu m$  square) is plotted against time. The relative stretch ratio is defined as the difference between the stretch ratio at the

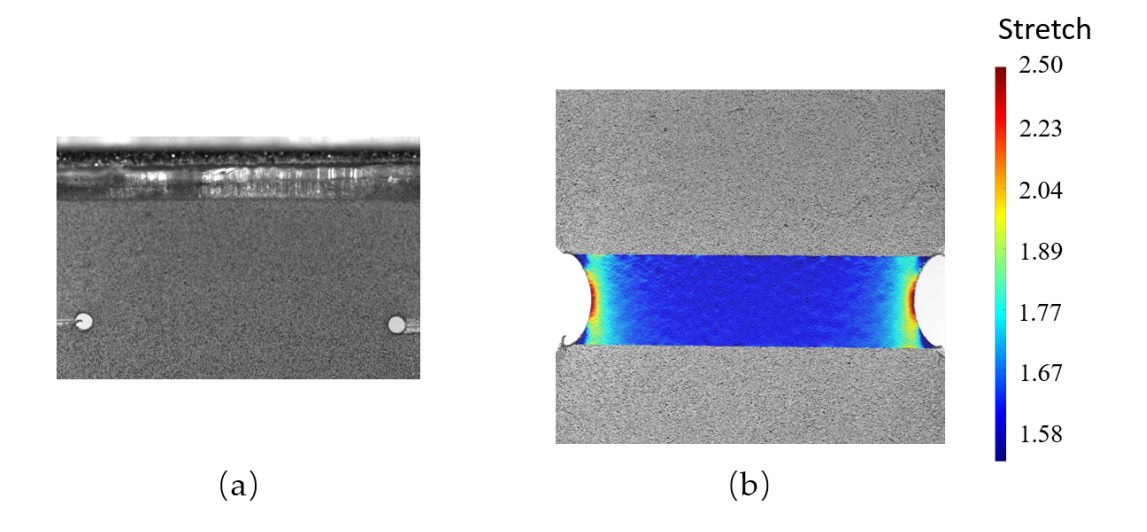


Figure 2: A blunt crack in a DEC specimen, only a small part of crack is shown due to limited field of view of camera.

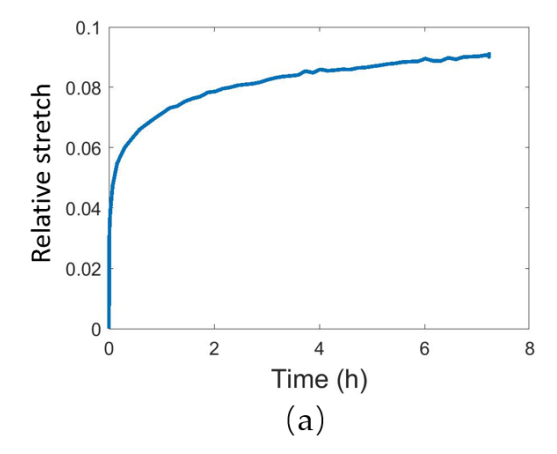
(a) Sample before stretch, (b) Stretch field at notches for a sample at a stretch ratio of 1.6.

current time and the stretch ratio at the start of holding. During relaxation, the crack gradually opens and the nominal strain (or stretch)  $\epsilon_{22}$  near the crack tip increases with time as well.

Fig. 3(a) shows that the stretch ratio increases very rapidly in the first few minutes, then increases very slowly over a period of 7 hours. This result is unexpected for PDMS. In our previous work, we see similar results in a PA gel, and we concluded that this phenomenon was caused by nonlinear viscoelasticity, where relaxation time decreases with strain [24]. However, the viscoelasticity of our PDMS should be small (see S1), and one would expect the relaxation time to be independent of strain. From our rheology test in SI and the rheology data from Placet et. al. [25], the loss modulus of PDMS does not reach its peak even when the frequency is  $10^5$ Hz, which means that the characteristic relaxation time of PDMS is smaller than  $10^{-5}s$ ; therefore, the duration of the viscoelastic change in strain should also be very small, roughly on the order of milliseconds; after this period, the strain should not change with time. This is clearly not the case in Fig. 3(a) where the strain keeps increasing for hours.

To further rule out the influence of viscoelasticity, we change the loading history in our experiment. One important feature of viscoelasticity is that strain is recoverable. If the increase in strain is due to viscoelasticity, then the entire sample should recover to its original unstrained state if we unload the sample to zero strain and let it relax for a time much longer than its characteristic relaxation time. This means that if we repeat the relaxation test after sufficient recovery time, the increase of strain should follow the same curve in Fig. 3(a). However, this is not what we observed in this experiment. After unloading and 1 hour of relaxation, we stretched the sample to 1.6 again and monitored its strain change during holding. We found that the strain at the beginning of this second holding is not the same as the initial strain of the first holding. Instead, it is almost the same as the

120



135

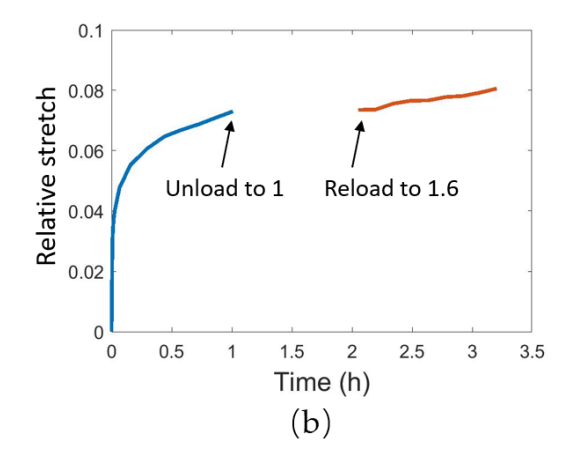


Figure 3: Time history of relative stretch at a fixed point near the blunt crack tip in a DEC specimen (a) Relative stretch increases near the blunt crack tip during hold. (b) History of relative stretch near the blunt crack tip. The sample is first loaded to a nominal stretch of 1.6, held for 1 hour, then unloaded rapidly to its original length ( $\lambda = 1$ ), then rest for one hour, then reload to a stretch ratio of 1.6. In both plots, t = 0 corresponds to the start of holding which in our experiments is 6s after the start of stretching.

strain at the end of the first holding - there is no recovery (Fig. 3(b)). This means that the strain increase near the crack tip is cumulative and not recoverable, thus cannot be due to viscoelasticity. Our hypothesis is that this increase in strain during relaxation is due to non-recoverable damage due to breaking of polymer chains near the crack tip. This hypothesis is consistent with the observation of Kooij et al. [9] and Ju et al. [8]. In the discussion, we will provide insight on how damage couples with the elastic field to yield the result in Fig. 3a.

The second interesting phenomenon is that the sample eventually breaks after a period of holding of about 7 hours. Unstable crack growth occurs in less than the 0.05s image acquisition period, thus we are unable to determine the crack growth history. However, before the sample broke, we managed to capture some interesting photos. Fig. 4 shows photos of the notch 1.8s - 0.05s before rapid fracture. We observe a small sharp wedge on the surface of the original blunt crack tip which grows during relaxation. When the length of this small wedge (or small crack) grows to about  $70\mu m$ , its rate of growth increases rapidly and a crack initiates and cuts across the sample in less than 0.05s. It should be noted that this "small crack" is linked to a much longer pre-existing blunt notch, hence it has much higher stress/strain than a small crack of length  $70\mu m$ . This observation is consistent with the observation of Kooij et al. [9]. These authors used laser speckle imaging to show the existence of an intense damage wedge region directly ahead of a blunt crack tip in PDMS seconds before catastrophic failure. At the end of section 4.3, we will provide a physical explanation for this observation.

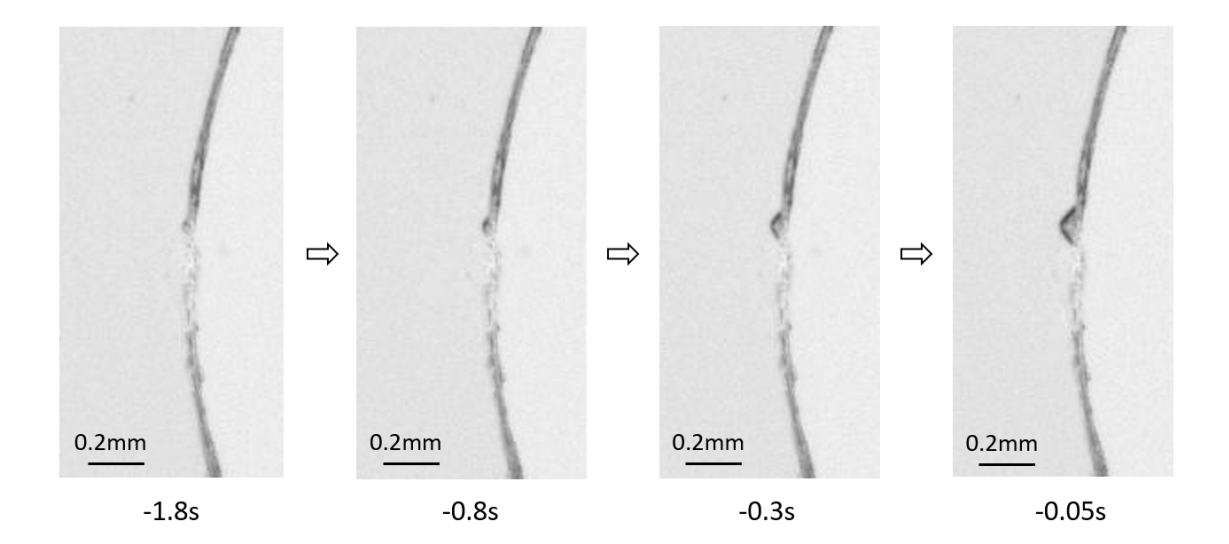


Figure 4: Small sharp crack nucleation before static delayed fracture. The dark line is the crack face and crack on the right side. Times shown are time before the start of unstable crack growth. To see the small crack clearly, there is no speckle pattern in this test.

## 3.2. Delayed fracture in sharp crack PS samples

The situation is very different for sharp crack tips. We first performed relaxation tests for a PS sample with a 10mm long sharp initial crack. We stretched the sample to  $\lambda = 1.12$  and then held the displacement. During holding, the load relaxes; nevertheless, the crack initiates and then propagates with a constant speed (see Fig. 5b). To study the dependence of crack growth rate, v, on the applied stretch ratio  $\lambda$ , additional relaxation tests are performed with the same specimen geometry but with different holding stretches. Fig. 5 shows that the crack growth rate, v, is nearly constant, for all tests, the higher the applied stretch ratio  $\lambda$ , the faster the v. The crack speed in Fig. 5 ranges over five order of magnitude, from v = 1nm/s ( $\lambda = 1.08$ ) to v = 0.1mm/s ( $\lambda = 1.16$ ).

#### 3.3. Constant stretch rate test

The relationship between v and  $\lambda$  is used to characterize DF of sharp cracks in PS samples. For such a relationship to be useful, it should be applicable to quasi-static crack growth (not only steady state) under different loading histories. To test our theory, we perform a test for the same PS crack sample with a constant stretch rate of  $10^{-4}/s$  until failure. During this test, we recorded the crack length from the acquired images and then calculated the crack growth rate by taking the derivative of the crack length versus time curve. Fig. 6 plots v against  $\lambda$  using this procedure. Also, the data from the four relaxation tests in Fig. 5 are plotted in Fig. 6 for comparison. The important result is that all data fall closely on a single curve. In addition, we found that this curve is independent of the stretch rate in our tests). This shows that there is a universal relation governing crack growth

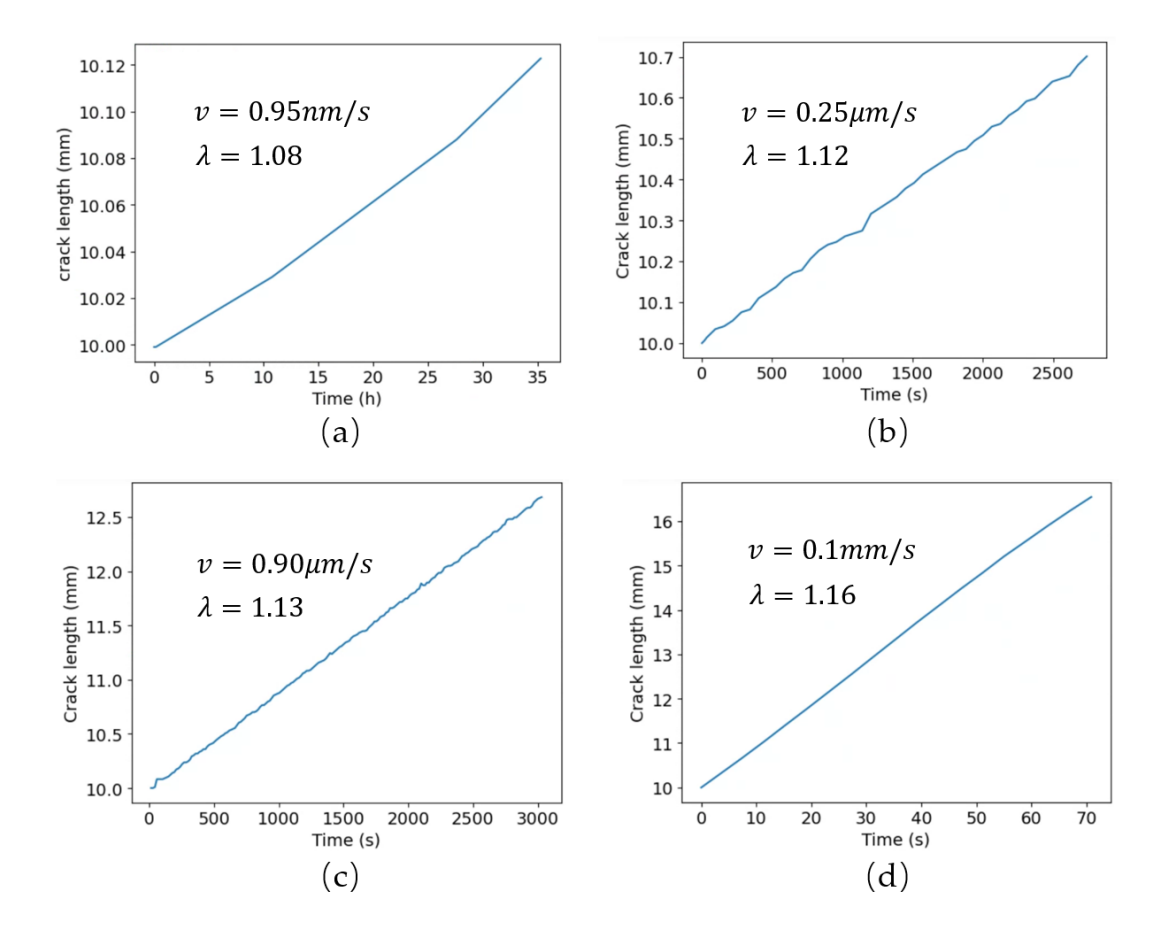


Figure 5: Crack length versus time in identical PS crack specimens subjected to different stretches: (a) 1.08, (b) 1.12, (c) 1.13, (d) +1.16. Zero time in these figures correspond to start of relaxation.

rate and applied stretch in a pure shear test, irrespective of the manner of loading, as long as the crack is growing in a quasi-static manner.

Our next step is to develop a model for crack propagation which is independent of specimen geometry. In this model, the applied stretch ratio  $\lambda$  in the PS tests is replaced by the energy release rate.

# 3.4. Fracture Mechanics: G controlled crack growth

We propose a model which relates the crack growth rate to energy release rate of a specimen with a sharp crack. The key assumption is small scale damage (SSD): that is, the region of damage is confined near the crack tip and is small in comparison with specimen geometry, specifically, c and H, where c is the crack length and H is the height of the strip. In a purely hyper-elastic solid, the true stress tensor near the crack tip is dominated by  $\sigma_{22}$  [26], the nominal stress in the loading direction, i.e.,

$$\sigma_{22} \sim \frac{\alpha J}{r} \tag{1}$$

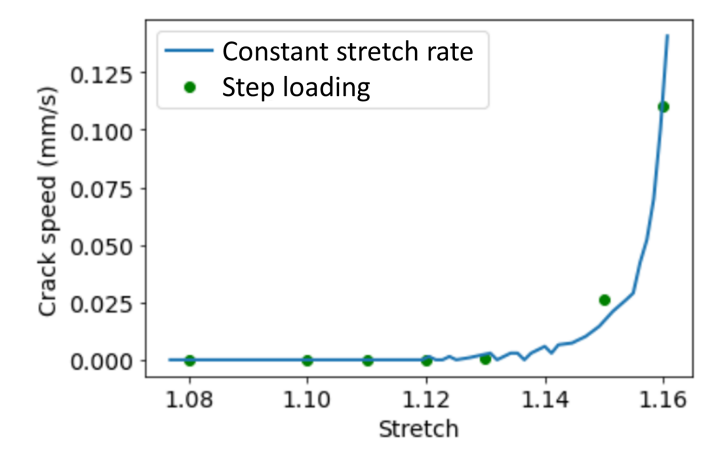


Figure 6: Steady crack propagation speed under different applied stretch ratios  $\lambda$ . Data are from two loading histories on PS specimens.

where J is the path independent J integral [27], r is the radial coordinate of a material point in the undeformed configuration, and  $\alpha$  is a numerical factor that depends on the angular coordinate and strain hardening characteristics. J is equal to energy release rate G in elastic solids. SSD implies that J is the unique parameter that controls damage. This means that, for SSD, there is a unique relationship between the crack speed to the applied energy release rate G. For an ideal PS specimen, the strip is infinitely long, and c >> H (semi-infinite crack), G is given by [28]

$$G_{PS} = W(\lambda)H\tag{2}$$

where W is the strain energy density function for material points in the PS geometry at large distances ahead of the crack tip. As shown below, in real PS samples, as long as the crack length is longer than H, the energy release rate is approximately independent of crack length and is given by Eq. (2). To determine the material constants in W, we perform uniaxial tension test of our PDMS using a dog-bone sample stretched at a rate of 0.1/s until failure (see S2 in supplementary information). We observe considerable strain hardening for strains over 30% and found that the tension behavior can be well fitted by a 3-term Yeoh's hyper-elastic model (see S2 in supplementary information). In this model, the strain energy density function for PS in Eq. (2) is:

$$W(\lambda) = \sum_{k=1}^{3} c_k (I_1 - 3)^k, \quad I_1 = \lambda^2 + \lambda^{-2} + 1$$
 (3)

The constants  $c_k$  in Eq. (3) have units of stress and are  $c_1 = 0.2216MPa$ ,  $c_2 = 4.4873 \times 10^{-2}MPa$  and  $c_3 = 6.9596 \times 10^{-3}MPa$ . The constant  $c_1$  is one half of the small strain shear modulus of the solid whereas  $c_2$  and  $c_3$  control strain hardening. Note that since the  $c_3$  term is proportional to  $\lambda^6$ , the strain energy density can be strongly affected by strain hardening. The special case where  $c_2 = c_3 = 0$  corresponds to a neo-Hookean solid.

## 3.5. FEM result for G in a PS specimen with short crack lengths

Eq. (2) is an exact result for an ideal PS specimen. Of course, specimens that are infinitely long with a semi-infinite crack cannot be made. Therefore, it is important to determine the true energy release rate in a real specimen. More importantly, to validate our model (see below), we need the relation of v versus G using different crack lengths, some of these are small in comparison with H. Specifically, we use the same specimen geometry except we use cracks of different lengths c. Fig. 7 plots the normalized energy release rate  $\overline{G} \equiv G/G_{PS}$  versus the normalized initial crack length  $\overline{c} \equiv c/H$ . The result in Fig. 7 is obtained using a finite element method (FEM) (see S5 for details).

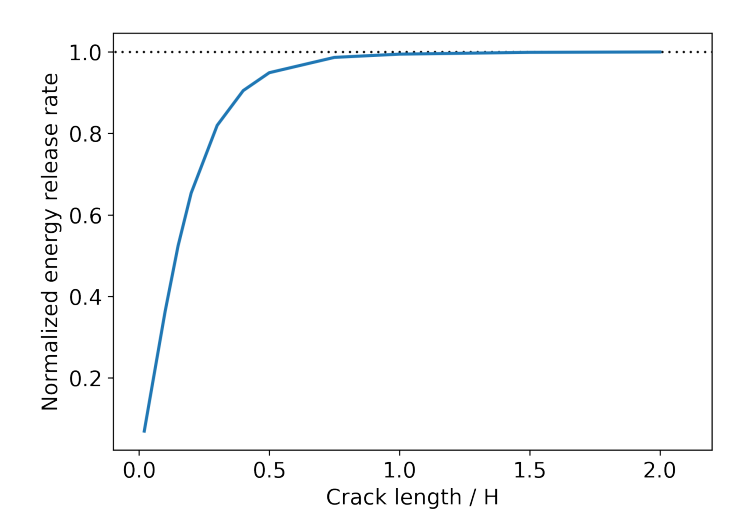


Figure 7: Normalized energy release rate (normalized by  $G_{PS}$  in Eq. (2)) versus normalized crack lengths for an applied stretch ratio 1.12 in a PS sample.

Recall that the length of our PS specimen is 35mm and the height H is 10mm. When the crack length c is between 10-20mm, the energy release rate G is practically independent of crack length and is given by Eq. (2) and Eq. (3). However, when c is less than 10mm, G decreases with decreasing crack length. Fig. 7 shows that when c/H < 0.2,  $G/G_{PS}$  increases linearly with c, i.e.,

$$G/G_{PS} = \omega c/H \Rightarrow G = \omega W(\lambda)c \qquad c/H < 0.2$$
 (4)

where  $\omega = 1.18\pi$ , which is the slope of the linear part in Fig. 7. It is important to note that  $G \propto W(\lambda)c$  for short cracks is a universal relation and can be obtained using a scaling or dimensional argument, as was done by Rivlin [28]. The proportional constant  $\omega$  is independent of crack length but can depend on the hyper-elasticity model. The result in Fig. 7 is for  $\lambda = 1.12$ . However, we found that the relation between normalized energy release rate  $G/G_{PS}$  and normalized crack length is practically independent of the stretch ratio.

This result shows that when the crack length is short, the specimen can no longer be considered as a pure shear crack specimen. Indeed, when  $c \ll H$ , the crack geometry approaches an edge crack

in an infinite plate. Fig. 7 or Eq. (4) shows that a larger applied stretch is needed to provide the same energy release rate for short cracks (as compared to crack longer than H). This information is provided in Fig. 8 where the orange curve is our FEM result which plots the stretches needed for different crack lengths to maintain the energy release rate of  $114.7J/m^2$ . If our assumption that the relation between v and G is unique is true, then cracks with different initial lengths but with the same  $G(114.7J/m^2)$  should have the same  $v = 0.25\mu m/s$ , which is measured in our experiment. To validate this, we performed experiments with different initial crack lengths and stretched them slowly until the crack propagation speed reaches about  $0.25\mu m/s$ . We recorded the stretch ratios at this time and plotted them as dots in Fig. 8. We then use FEM to compute the stretch needed to get  $G = 114.7J/m^2$ , that is, a constant energy release rate curve. The experimental data is very close to this constant energy release rate curve, which validates the unique relation between v and G.

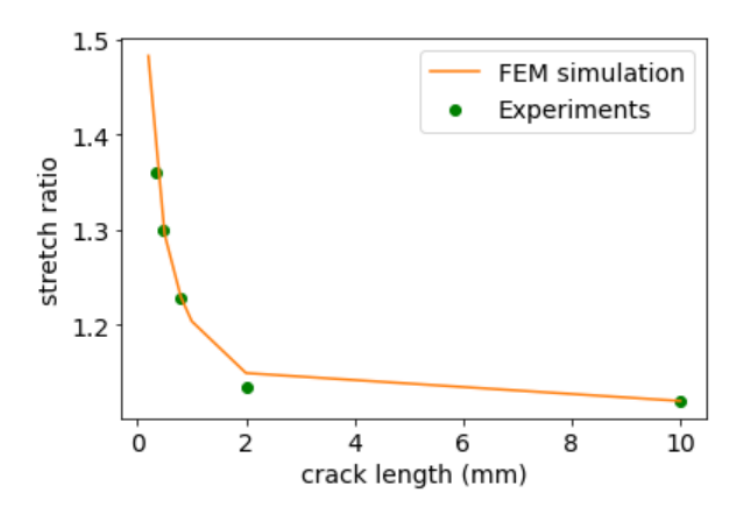


Figure 8: Applied stretch ratios for different crack lengths at a constant crack speed of  $0.25\mu m/s$ . These stretch ratios correspond to the energy release rate of  $114.7J/m^2$ 

## 3.6. Crack speed versus G

205

Having established that the crack speed v is a unique function of G, we plot v versus G(Fig. 9) for the long crack experiments and see that it is a straight line in semi-log scale and thus that v is exponential with G. Our computational analysis below will be used to fit v as an exponential function of G, i.e. to fit

$$v = v^* e^{G/G^*} \tag{5}$$

An important feature not shown in Fig. 9 is that we observe a threshold energy release rate below which the crack does not grow. In our experiments, when the energy release rate is lower than  $35J/m^2$ , no crack propagation is observed even after 48 hours of holding. However, this could be due to the spatial resolution  $(6\mu m)$  of our measurement technique or that longer time is required.

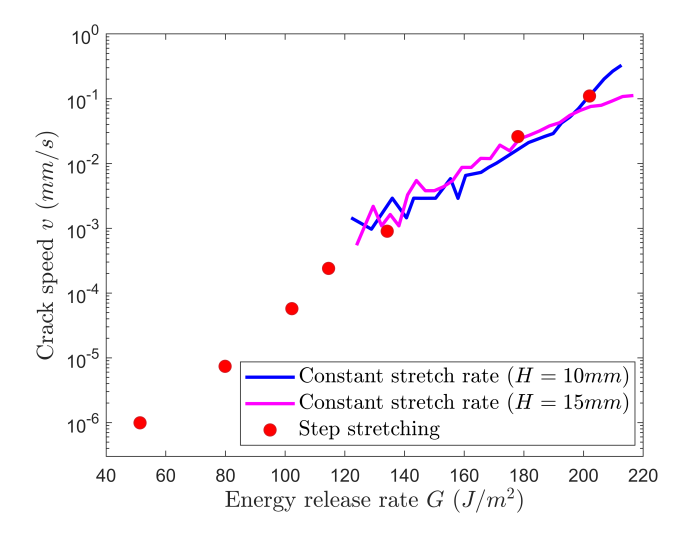


Figure 9: Crack speed versus energy release rate. The experiments with constant  $\dot{\lambda}$  were repeated for PS samples with H=15mm, also at  $\dot{\lambda}=10^{-4}/s$ . The good agreement between H=10mm and H=15mm provides further support for the dependence of v on G.

#### 4. Modelling v versus G

# 4.1. Time-dependent damage model

Our experimental observations show that there exists a unique relation between v and G given by Eq. (5). Although the exponential function fits the experimental data very well, it is still a phenomenological result. Here we propose a physical model to explain the origin of this exponential relationship. Our experimental results suggest that the delayed fracture behaviors of PDMS are due to the time-dependent permanent damage of polymer chains in a region near the crack tip. The basic theory of rate dependent chain scission was established by Eyring [29] and his model has been incorporated into a cohesive zone model to study rate dependent fracture in polymers [30]. Here we adopt the formulation of Lavoie et al [31]. In their formulation, the polymer elasticity is represented by many networks, the chains in each network have equal lengths. To avoid having a large number of undetermined parameters in our model, we consider a simple network where chains have equal length, hence the length of chains is an average length in the real network. In this model, the surviving volume fraction of polymer chains is denoted by b, and the rate of change of b is given by

$$\frac{db}{dt} = -\frac{n_m}{\tau} b \exp\left(\frac{L_a f}{k_B T}\right) \tag{6}$$

where  $\tau$  represents the relaxation time for bond dissociation,  $L_a$  is the activation length which is assumed to be constant [31],  $n_m$  is the number of monomers in a chain, f is the force acting on a polymer chain,  $k_B$  is the Boltzmann's constant and T is the absolute temperature in Kelvin.

In [31], the relation between the chain force f and the extension of a chain is determined using the freely jointed chain model. The extension of a chain is computed based on the affine assumption

where the extension of each chain in the network is obtained from the local deformation gradient  $\mathbf{F}$ . Using the Arruda-Boyce constitutive model, f is related to  $I_1 = tr(\mathbf{B})$ , where  $\mathbf{B}$  is the left Cauchy-Green tensor, by [31]:

$$f = \frac{k_B T}{l_L} \beta \left( \sqrt{I_1(\mathbf{B})/3n} \right) \tag{7}$$

where  $l_k$  is the Kuhn length of the polymer chain, n is the number of Kuhn segments per chain and  $\beta\left(\sqrt{I_1(B)/3n}\right)$  denotes the inverse Langevin function defined by

$$\coth\beta - \frac{1}{\beta} = \sqrt{I_1(\mathbf{B})/3n} \tag{8}$$

However, the use of the Arruda-Boyce model in [31] is inconvenient in that the inverse Langevin function cannot be written in closed form. Here we introduce a simplification by using an approximation of the Langevin function [32] (less than 5% relative error everywhere) where

$$\beta\left(\sqrt{I_1(\mathbf{B})/3n}\right) \approx \left(\sqrt{I_1(\mathbf{B})/3n}\right) \left[\frac{3 - I_1(\mathbf{B})/3n}{1 - I_1(\mathbf{B})/3n}\right]$$
(9)

Substituting Eq. (9) into Eq. (7) shows that the chain force is related to the deformation by

$$f = \frac{k_B T}{l_k} \sqrt{I_1(\mathbf{B})/3n} \left[ \frac{3 - I_1(\mathbf{B})/3n}{1 - I_1(\mathbf{B})/3n} \right]$$
 (10)

The chain breaking kinetics Eq. (6) can be expressed in terms of continuum quantities by substituting Eq. (10) into Eq. (6), resulting in

$$\frac{db}{dt} = -\frac{n_m}{\tau} b \exp\left(\frac{L_a}{l_k} \sqrt{\frac{I_1(\mathbf{B})}{3n}} \left[ \frac{3 - I_1(\mathbf{B})/3n}{1 - I_1(\mathbf{B})/3n} \right] \right)$$
(11)

In this model, damage takes time to develop. However, due to the exponential function in Eq. (11), the rate of damage increases exponentially fast as a chain reaches the limit of its extensibility. In the continuum model, this occurs when  $I_1(\mathbf{B}) \to 3n$ , and db/dt becomes unbounded.

## 4.2. Calculating crack propagation speed using Chain Damage Model

In the following, we determine the relation between crack growth rate v and the applied energy release G rate in a PS specimen using a simple analytic model. We assume steady state crack growth. Under this assumption, the continuum field is independent of time with respect a coordinate system (x, y) fixed to the moving crack tip in the reference configuration with x parallel and y perpendicular to the crack. The steady state assumption implies that the material derivative of b, Db/Dt is given by

$$\frac{Db}{Dt} = -v\frac{\partial b}{\partial x} \tag{12}$$

where v is the speed of the crack, b = b(x, y) in the moving coordinate system. Substituting Eq. (12) into Eq. (11), we have

$$v\frac{\partial b}{\partial x} = \frac{n_m}{\tau} b \exp\left(\frac{L_a}{l_k} \sqrt{\frac{I_1(\mathbf{B})}{3n}} \left[ \frac{3 - I_1(\mathbf{B})/3n}{1 - I_1(\mathbf{B})/3n} \right] \right)$$
(13)

A difficulty with the damage model of Eq. (13) is that healing is neglected, hence damage occurs irrespective of the stress/strain level. While this assumption is reasonable near the crack tip, it is incompatible with the steady state assumption since the material as  $x \to \infty$  is undamaged. To by-pass this difficulty, we introduce a cut-off effective strain, represented by  $I_c$ , such that the damage rate is zero for  $I_1 \le I_c$ . In Eq. (14), the upper limit of integral L corresponds to the distance from the crack tip to the position directly ahead of the crack tip where  $I_1$  reaches  $I_c$ . We also impose the fracture condition that crack growth occurs when the damage reaches a critical fraction  $b_c$  at a microscopic distance  $x_c$  directly ahead of the crack tip. These assumptions allow us to integrate Eq. (13) directly ahead of the crack tip (y = 0) to yield

$$v = \frac{n_m}{\tau \ln(1/b_c)} \int_{x_c}^{L} \exp\left(\frac{L_a}{l_k} \sqrt{\frac{I_1(\boldsymbol{B}(y=0,x))}{3n}} \left[ \frac{3 - I_1(\boldsymbol{B}(y=0,x))/3n}{1 - I_1(\boldsymbol{B}(y=0,x))/3n} \right] \right) dx$$
(14)

To complete the analysis, we need to know how  $I_1(\mathbf{B}(y=0,x))$  varies with x. In general, this strain field is coupled to the damage. To simplify the analysis, we assume the damage zone is sufficiently small so that the strain field is the same as a long crack in a hyper-elastic PS sample obeying the 3 term Yeoh's model (Eq. (3)). The strain field is determined by a simulation using Abaqus (see S6). Since the PS specimen is under displacement control, the effect of damage is reflected in the stress field instead of the strain field, so the hyper-elastic strain field should provide a good approximation of the actual strain field.

There are 5 independent parameters in our model,  $\{\tau \ln(b_c)/n_m, x_c, I_c, n, L_a/l_k\}$  and we choose these parameters by randomly searching 1 million points in the parameter space to fit the experimental data. The results are shown in Fig. 10. The figure shows that the model can predict the crack speed observed in experiments quantitatively. The parameters are

$$\{\tau \ln(b_c)/n_m, x_c, I_c, n, L_a/l_k\} = \{-208.7s, 8.9\mu m, 4.155, 2.021, 1\}$$
(15)

# 4.3. Delayed fracture in PS samples with short initial crack lengths

We are now ready to analyze how crack geometry controls DF. To recap, sharp cracks in PS samples fail at lower stretch ratios than in DEC samples. The mode of failure is slow, steady crack growth. We emphasize that these experiments are conducted with cracks longer than sample height H. In contrast, blunt crack samples fail at higher stretch ratios and the failure mode is sudden rapid crack growth, similar to the observation of [9]. Superficially, it seems that these two phenomena are unconnected. In the following, we show that the underlying failure mechanism is the same and they can be understood using the same model.

We first present data on DF tests with very short sharp cracks (c = 0.8 - 0.34mm) in PS samples. The samples are stretched to  $\lambda = 1.23 - 1.30$  at a stretch rate 0.1/s and then held fixed. Note these

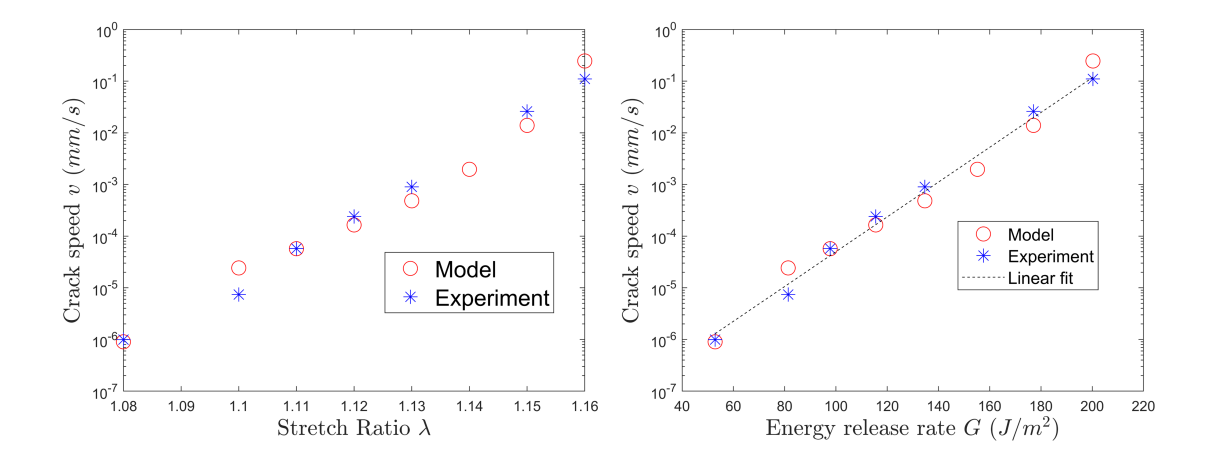


Figure 10: Fitting result of polymer chain damage model. (a) Crack growth speed versus stretch. (b) Crack growth speed versus energy release rate. Using Eq. (5), the linear fit of the damage model results is shown as a dashed line on a semi-log scale. Here we have  $v^* = 2.144 \times 10^{-8} mm/s$ ,  $G^* = 12.896 J/m^2$ .

stretch ratios are much larger than those needed to grow a long starter crack. Photos are taken during holding and the time evolution of crack length is recorded. As shown in Fig. 11(a)-(d), the crack propagates very slowly at first, but the crack speed keeps increasing. In Fig. 11 (a), after 400 seconds, the crack speed suddenly increases rapidly and breaks the sample in less than 3 additional seconds.

The crack length evolution can be explained using a simple physical argument. Initially, the crack length is very short and since the energy release rate is directly proportional to the crack length (see Fig. 7), it is also very small. A small energy release rate means slow crack growth rate, as predicted by our model, Eq. (1) (see also Fig. 9 and Fig. 10). Once the crack grows, the crack length increases, which leads to the increase of energy release rate. A higher energy release rate, in turn, results in a faster crack speed. This positive feedback, combined with the exponential dependence of crack speed on G, causes the crack to grow increasingly faster, eventually leading to the catastrophic failure of the sample. This argument will be justified rigorously below.

In Fig. 11(a), the crack speed seems to approach infinity when the crack length is slightly below 1.5mm (short crack). This is the case for all the initial crack lengths in Fig. 11. Hence the energy release rate in these experiments is given by Eq. (4). Using Eq. (4), Eq. (5) and v = dc/dt. The rate of change of crack length for short cracks obeys the differential equation

$$\frac{dc}{dt} = v^* e^{W(\lambda)\omega c/G^*} \tag{16}$$

The solution of Eq. (16) subjected to the initial condition  $c(t = 0) = c_0$  where  $c_0$  is the initial crack length. Then c(t) is

$$c(t) = c_0 - \frac{G^*}{W(\lambda)\omega} \ln\left(1 - \frac{t}{t_{max}}\right)$$
(17)

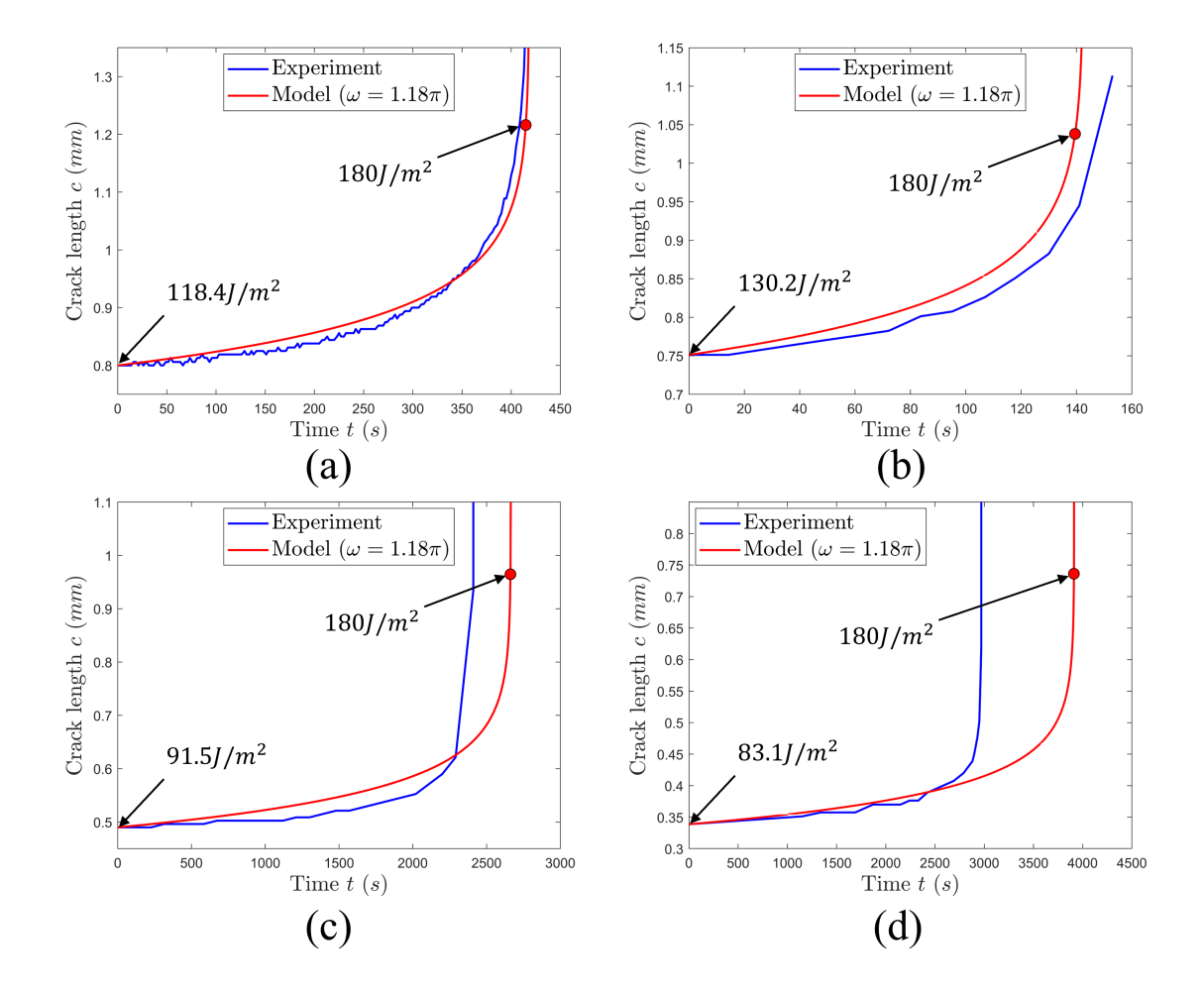


Figure 11: Delayed fracture tests on sharp crack samples for four initial crack lengths. (a)  $c_0 = 0.80mm$  crack with stretch  $\lambda = 1.23$ , (b)  $c_0 = 0.75mm$  crack with stretch  $\lambda = 1.25$ , (c)  $c_0 = 0.49mm$  crack with stretch  $\lambda = 1.26$ , (d)  $c_0 = 0.34mm$  crack with stretch  $\lambda = 1.30$ . The theoretical results are calculated using Eq. (17). Here  $v^* = 2.144 \times 10^{-8}mm/s$  and  $G^* = 12.896J/m^2$ , which are given by the linear fit of the damage model in Fig. 10. Recall  $\omega = 1.18\pi$ , which is the slope of the linear part in Fig. 7. Energy release rate values noted on the figures refer to G for the starter crack at the indicated stretch and  $G = 180J/m^2$ , the approximate G value at this the crack begins to grow unstably.

where

$$t_{max} = \frac{G^* e^{-G_0/G^*}}{G_0} \frac{c_0}{v^*} \tag{18}$$

and

$$G_0 = \omega W(\lambda) c_0 \tag{19}$$

is the energy release rate of the initial crack. The dependence of crack growth rate on time is obtained by differentiating Eq. (17), i.e.,

$$v = \frac{dc}{dt} = \frac{G^*}{G_0} \frac{1}{1 - t/t_{max}} \frac{c_0}{t_{max}}$$
 (20)

Note that the crack growth rate approaches infinity as t approaches  $t_{max}$ . Eq. (20) captures the rapid increase of crack velocity at finite time in Fig. 11. The predicted crack length using Eq. (17), Eq. (18) and Eq. (19) fits the experimental crack length well.

One interesting feature in all four tests is that the rapid increase in crack speed occurs at roughly the same energy release rate ( $\sim 180 J/m^2$ ). From Fig. 9 and Fig. 10, we can see that at this energy release rate, the crack speed reaches 0.01 mm/s. In all these short crack tests, the cracks grow only 0.1 - 0.5 mm before catastrophic failure occurs.

These results provide a simple explanation of why rapid crack growth is associated with delayed fracture in blunt crack specimens. Specifically, very small cracks nucleated directly ahead of the notch tip in blunted crack specimens propagate slowly, and are not easily observable (see Fig. 4), but once they reach a certain size  $(70\mu m)$ , they can accelerate rapidly since the energy release rate is very high due to the presence of the pre-existing notch. Note that the energy release rate is high because the applied stretch ratio is much higher than the applied stretch ratio for cracks of the same length in the PS samples, due to lower stress concentration.

### 5. Summary and Discussion

275

280

A study for the delayed fracture of PDMS is carried out to study DF in different crack specimens containing sharp and blunted cracks. Our experiments showed that DF is caused by localized damage due to rate dependent bond breaking. In blunted crack samples, DF occurs at higher energy release rate and crack growth following initiation is catastrophic. In contrast, in sharp crack samples with sufficiently long cracks, DF occurs at much lower energy release and crack growth is slow and steady. Experimentally, we found that the velocity of crack growth is uniquely related to the energy release rate. In particular, the crack velocity is an exponential function of the energy release rate. We also derive this v versus G relation using a fracture model based on rate dependent chain breaking kinetics and found good agreement between theory and experiments.

Our experiments and theory provide strong evidence that DF in samples with blunted and sharp cracks are governed by the same micromechanics of chain breaking. Once a small crack is formed in blunted samples, the crack growth rate can be explained by the universal relation between crack growth rate and energy release rate given by Eq. (5). In other words, DF can be explained by combining chain breaking kinetics with concepts from nonlinear fracture mechanics.

The result in Fig. 3 (a) can be explained by the interaction between chain breaking and elastic field. Fig. 3 (a) shows that the stretch at a fixed point directly ahead of the blunted tip increases very rapidly for the first few minutes after holding and then continues to increase at a much slower rate. In a purely elastic solid, this increase is impossible since the strain distribution is fixed and cannot change with time during holding. The cause of this increase is due to time-dependent damage caused by chain breaking. Indeed, our damage model implies that damage softens the material by decreasing

the effective shear modulus  $2c_1$  to  $b \times 2c_1$  (recall  $2c_1$  is the shear modulus in Yeoh's model and b is the volume fraction of unbroken chains). This means that there is a region of softened material near the notch tip, surrounding this softened region is undamaged material which is substantially stiffer. Since the average spatial strain during relaxation must be constant, strain is transferred to the softer material near the notch tip, as a result, the strain of the material near the notch tip increases, this increase in strain is compensated by equal decrease of average strain in the surrounding stiffer solid. To understand the rapid increase in strain, we appeal to the fact that the network strands in PDMS have a wide molecular weight distribution. Consequently, the short strands break rapidly due to the strain concentration near the notch tip. After this initial period of rapid breaking, all the short strands are broken. The remaining long strands require much higher strain to break rapidly, but can gradually break as they are aided by thermal fluctuation. This explains the slow increase in strain over hours.

Our crack growth model, as represented by Eq. (14), simplifies many aspects of the network. In our model, we assume the network consists of chains of the same length. However, in a real network, there is a variation in chain lengths, with shorter chains being much more prone to breaking. Additionally, our damage model relies on an affine approximation, which assumes all chains at a given material point experience the same deformation field. While this assumption holds for minor damage, it becomes inaccurate near the crack tip because the network's structure changes as damage occurs. Therefore, the specific details of our damage model can substantially affect the length scale, denoted as  $x_c$  in Eq. (14). Consequently, it's crucial to be careful when interpreting the parameters in Eq. (15) because they are affected by these simplifications and assumptions.

An interesting issue raised by this work is the meaning of fracture toughness for materials with time-dependent damage, like PDMS. In fracture mechanics, the toughness is the minimum energy release rate required to initiate crack growth so it should correspond to the energy release rate below which crack growth rate is zero. However, in most experiments measuring toughness, this value is usually obtained by stretching a PS sample with constant loading rate until the crack length has a noticeable increase. This toughness is much higher than the critical energy release rate for crack growth we observed, which is around  $35J/m^2$ . In theory, there is a critical energy release rate, i.e., the surface energy, below which crack growth cannot occur. For PDMS, the surface energy has been measured [33] and is found to be  $21.6mJ/m^2$ . Thus, this "critical" energy release rate must be greater than  $43.2mJ/m^2$ , which is unrealistically small. As noted by Lake and Thomas (LT)[34], the toughness of elastomers is much greater than its surface energy since when a chain breaks, it loses all its strain energy.

In LT theory [34], toughness is given by the product of the number of effective load bearing chain crossings per unit reference area, of the average number of monomers per chain and of the energy needed to break the chemical bond between monomers. LT [34] shows that this fracture energy is

given by  $\Gamma_{LT} = \sqrt{3/8} \gamma l U \xi$ , where l is the monomer length,  $\gamma$  is a factor determined by the freedom of rotation about bonds in the chain which influences the flexibility, which we take to be one, U is the energy needed to break a polymer bond and  $\xi = N \overline{n}^{3/2}$ , where  $\overline{n}$  is the number of monomer unit in a chain, and N is the number of effective load bearing chains per unit volume. N can be obtained using polymer physics [35]. For PDMS, our estimation for N is

$$N = \frac{\mu}{kT} = \frac{0.44 \times 10^6 Pa}{4.11 \times 10^{-21} J} \approx 10^{26} / m^3$$
 (21)

where  $\mu = 2c_1$  (see Eq. (3)) is the small strain shear modulus.

The average number of monomer units per chain is

$$\overline{n} \approx \frac{\rho}{mN}$$
 (22)

where m is the mass of a single monomer unit and  $\rho$  the mass density. The repeated unit of PDMS is Si (CH<sub>3</sub>)<sub>2</sub> O and the mass density is  $965kg/m^3$ . Thus, the mass per monomer is about  $1.27 \times 10^{-25}kg$ . This gives

$$\overline{n} = \frac{\rho}{mN} = \frac{965kg/m^3}{1.27 \times 10^{-25}kg \times 10^{26}/m^3} \approx 80 \tag{23}$$

For this we can find

$$\xi = N\overline{n}^{3/2} \approx (80)^{3/2} \times 10^{26} / m^3 \tag{24}$$

Taking the monomer length of PDMS to be 10 Angstroms, the toughness predicted by LT is

$$\Gamma_{LT} = \sqrt{3/8} \gamma l U \xi \approx \sqrt{3/8} \times 10 \times 10^{-10} m \times 3 \times 10^{-19} J \times 10^{26} / m^3 \times (80)^{3/2} = 13.1 J / m^2 \quad (25)$$

This is the lower bound for the threshold "fracture toughness", since it assumes all the damage is confined to a single plane directly ahead of the crack tip. Thus, if the threshold energy for crack growth exists, it should be higher or equal to LT energy. In our experimental observations, the threshold energy for crack propagation is about  $35J/m^2$ , roughly two times higher than the LT energy.

It should be noted that in this study, the crack length is always much greater than the damage zone size or the radius of the blunted crack, this is the reason why fracture mechanics is applicable. If the size of the damage zone is comparable to the crack length, DF can no longer be governed by a single parameter, G. In the literature, this corresponds to samples that are notch insensitive [1, 36]. A key length scale proposed to quantify notch sensitivity is the fracto-cohesive length  $l_f = \Gamma/W_f$  [36], where  $\Gamma$  is the fracture toughness of the material and  $W_f$  is its work of extension which is the energy per unit volume to fail an uncracked tension sample. If the crack length is smaller than  $\Gamma/W_f$ , the sample is notch insensitive and fracture mechanics approach is not valid. For PDMS in this study,  $l_f$  is estimated to be  $13\mu m$  (with  $\Gamma = 35J/m^2$  and  $W_f = 2.69MPa$ , see S2), which is of the same order of magnitude of fit of our model. For sharp crack samples, using Eq. (16), when we have a  $18\mu m$  initial crack, a nominal stretch ratio of 2.5 is needed to reach a crack speed

0.01mm/s, which is very close to the fracture stretch ratio of 2.6 in uniaxial tension test. Here we note another length scale in soft material fracture is the elasto-adhesive length  $l_e = \Gamma/E$  [37, 38], where E is the small strain Young's modulus. This length represents the typical distance from a crack tip below which the deformation is dominated by elastic nonlinearity at the onset of crack initiation [38]. Thus, fracture mechanics cannot be applied if the damage zone size is on the same order as  $\Gamma/E$ . Interestingly, for our PDMS system, E = 1.3MPa,  $l_e = \Gamma/E \approx 26\mu m$  which is roughly the same order as the fracto-cohesive length.

#### Acknowledgement

This work is supported by the National Science Foundation, under Grant No. CMMI-1903308.

#### References

350

- [1] C. Chen, Z. Wang, Z. Suo, Flaw sensitivity of highly stretchable materials, Extreme Mechanics Letters 10 (2017) 50–57.
  - [2] S. Hassan, J. Kim, Z. Suo, Polyacrylamide hydrogels. iv. near-perfect elasticity and ratedependent toughness, Journal of the Mechanics and Physics of Solids 158 (2022) 104675.
  - [3] Y. Tanaka, R. Kuwabara, Y.-H. Na, T. Kurokawa, J. P. Gong, Y. Osada, Determination of fracture energy of high strength double network hydrogels, The Journal of Physical Chemistry B 109 (23) (2005) 11559–11562.
    - [4] X. Zhao, Multi-scale multi-mechanism design of tough hydrogels: building dissipation into stretchy networks, Soft matter 10 (5) (2014) 672–687.
    - [5] X. Wang, W. Hong, Delayed fracture in gels, Soft Matter 8 (31) (2012) 8171–8178.
- [6] S. Mzabi, D. Berghezan, S. Roux, F. Hild, C. Creton, A critical local energy release rate criterion for fatigue fracture of elastomers, Journal of Polymer Science Part B: Polymer Physics 49 (21) (2011) 1518–1524.
  - [7] R. Bai, J. Yang, Z. Suo, Fatigue of hydrogels, European Journal of Mechanics-A/Solids 74 (2019) 337–370.
- [8] J. Ju, G. E. Sanoja, M. Y. Nagazi, L. Cipelletti, Z. Liu, C.-Y. Hui, M. Ciccotti, T. Narita, C. Creton, Fast detection of early-stage damage in soft elastomers, In sumbission (2023).
  - [9] H. M. van der Kooij, S. Dussi, G. T. van de Kerkhof, R. A. Frijns, J. van der Gucht, J. Sprakel, Laser speckle strain imaging reveals the origin of delayed fracture in a soft solid, Science advances 4 (5) (2018) eaar1926.

- <sup>365</sup> [10] Y. Yu, N. Bouklas, C. M. Landis, R. Huang, Poroelastic effects on the time-and rate-dependent fracture of polymer gels, Journal of Applied Mechanics 87 (3) (2020).
  - [11] S. Pearson, Delayed fracture of sintered alumina, Proceedings of the Physical Society. Section B 69 (12) (1956) 1293.
  - [12] N. Petch, P. Stables, Delayed fracture of metals under static load, Nature 169 (1952) 842–843.
- [13] O. Lengliné, R. Toussaint, J. Schmittbuhl, J. E. Elkhoury, J. Ampuero, K. T. Tallakstad, S. Santucci, K. J. Måløy, Average crack-front velocity during subcritical fracture propagation in a heterogeneous medium, Physical Review E 84 (3) (2011) 036104.
  - [14] D. Bonn, H. Kellay, M. Prochnow, K. Ben-Djemiaa, J. Meunier, Delayed fracture of an inhomogeneous soft solid, Science 280 (5361) (1998) 265–267.
- [15] P. J. Skrzeszewska, J. Sprakel, F. A. de Wolf, R. Fokkink, M. A. Cohen Stuart, J. van der Gucht, Fracture and self-healing in a well-defined self-assembled polymer network, Macromolecules 43 (7) (2010) 3542–3548.
  - [16] J. Tang, J. Li, J. J. Vlassak, Z. Suo, Fatigue fracture of hydrogels, Extreme Mechanics Letters 10 (2017) 24–31.
- [17] S. N. Karobi, T. L. Sun, T. Kurokawa, F. Luo, T. Nakajima, T. Nonoyama, J. P. Gong, Creep behavior and delayed fracture of tough polyampholyte hydrogels by tensile test, Macromolecules 49 (15) (2016) 5630–5636.
  - [18] Y. Yang, H. Guo, Z. Du, W. Hong, T. Lu, T. Wang, Rate-dependent fracture of hydrogels due to water migration, Journal of the Mechanics and Physics of Solids 167 (2022) 105007.
- [19] K. Cui, Y. N. Ye, C. Yu, X. Li, T. Kurokawa, J. P. Gong, Stress relaxation and underlying structure evolution in tough and self-healing hydrogels, ACS Macro Letters 9 (11) (2020) 1582– 1589.
  - [20] Y. Mao, L. Anand, A theory for fracture of polymeric gels, Journal of the Mechanics and Physics of Solids 115 (2018) 30–53.
- [21] A. Kaminsky, Mechanics of the delayed fracture of viscoelastic bodies with cracks: Theory and experiment, International Applied Mechanics 50 (2014) 485–548.
  - [22] M. K. Chaudhury, Rate-dependent fracture at adhesive interface, The Journal of Physical Chemistry B 103 (31) (1999) 6562–6566.
- [23] T. L. Sun, T. Kurokawa, S. Kuroda, A. B. Ihsan, T. Akasaki, K. Sato, M. A. Haque, T. Nakajima, J. P. Gong, Physical hydrogels composed of polyampholytes demonstrate high toughness and viscoelasticity, Nature materials 12 (10) (2013) 932–937.

- [24] J. Wang, K. Cui, B. Zhu, J. P. Gong, C.-Y. Hui, A. T. Zehnder, Load transfer between permanent and dynamic networks due to stress gradients in nonlinear viscoelastic hydrogels, Extreme Mechanics Letters 58 (2023) 101928.
- [25] V. Placet, P. Delobelle, Mechanical properties of bulk polydimethylsiloxane for microfluidics over a large range of frequencies and aging times, Journal of Micromechanics and Microengineering 25 (3) (2015) 035009.
  - [26] R. Long, V. R. Krishnan, C.-Y. Hui, Finite strain analysis of crack tip fields in incompressible hyperelastic solids loaded in plane stress, Journal of the Mechanics and Physics of Solids 59 (3) (2011) 672–695.

405

420

- [27] J. R. Rice, A path independent integral and the approximate analysis of strain concentration by notches and cracks, Journal of Applied Mechanics 35 (1968) 379–386.
- [28] R. Rivlin, A. G. Thomas, Rupture of rubber. i. characteristic energy for tearing, Journal of polymer science 10 (3) (1953) 291–318.
- [29] A. Tobolsky, H. Eyring, Mechanical properties of polymeric materials, The Journal of chemical physics 11 (3) (1943) 125–134.
  - [30] J. Guo, A. T. Zehnder, C. Creton, C.-Y. Hui, Time dependent fracture of soft materials: linear versus nonlinear viscoelasticity, Soft Matter 16 (26) (2020) 6163–6179.
- [31] S. R. Lavoie, R. Long, T. Tang, A rate-dependent damage model for elastomers at large strain,
   Extreme Mechanics Letters 8 (2016) 114–124.
  - [32] A. Cohen, A padé approximant to the inverse langevin function, Rheologica acta 30 (1991) 270–273.
  - [33] M. K. Chaudhury, G. M. Whitesides, Direct measurement of interfacial interactions between semispherical lenses and flat sheets of poly (dimethylsiloxane) and their chemical derivatives, Langmuir 7 (5) (1991) 1013–1025.
  - [34] G. Lake, A. Thomas, The strength of highly elastic materials, Proceedings of the Royal Society of London. Series A. Mathematical and Physical Sciences 300 (1460) (1967) 108–119.
  - [35] M. C. Boyce, E. M. Arruda, Constitutive models of rubber elasticity: a review, Rubber chemistry and technology 73 (3) (2000) 504–523.
- [36] C. Yang, T. Yin, Z. Suo, Polyacrylamide hydrogels. i. network imperfection, Journal of the Mechanics and Physics of Solids 131 (2019) 43–55.

- [37] C.-Y. Hui, S. Bennison, J. Londono, Crack blunting and the strength of soft elastic solids, Proceedings of the Royal Society of London. Series A: Mathematical, Physical and Engineering Sciences 459 (2034) (2003) 1489–1516.
- <sup>430</sup> [38] C. Creton, M. Ciccotti, Fracture and adhesion of soft materials: a review, Reports on Progress in Physics 79 (4) (2016) 046601.